



OPEN

Real-Time Discrimination between Proliferation and Neuronal and Astroglial Differentiation of Human Neural Stem Cells

SUBJECT AREAS:
BIOPHYSICAL METHODS
NEURAL STEM CELLS

Received
24 February 2014

Accepted
19 August 2014

Published
10 September 2014

Rimi Lee¹, Il-Sun Kim², Nalae Han³, Seokhwan Yun⁴, Kook In Park^{2,4} & Kyung-Hwa Yoo³

¹Center for Nanosafety Metrology, Korea Research Institute of Standards and Science Daejeon, Republic of Korea, ²Division of Neonatology, Severance Childrens's Hospital, Department of Pediatrics, Yonsei University College of Medicine, Seoul, 120-752, Republic of Korea, ³Department of Physics, Yonsei University, Seoul, 120-749, Republic of Korea, ⁴BK21 Plus Project for Medical Science, Yonsei University College of Medicine, Seoul, 120-752, Republic of Korea.

Correspondence and requests for materials should be addressed to K.H.Y. (khyoo@yonsei.ac.kr) or K.I.P. (kipark@yuhs.ac)

Neural stem cells (NSCs) are characterized by a capacity for self-renewal, differentiation into multiple neural lineages, all of which are considered to be promising components for neural regeneration. However, for cell-replacement therapies, it is essential to monitor the process of *in vitro* NSC differentiation and identify differentiated cell phenotypes. We report a real-time and label-free method that uses a capacitance sensor array to monitor the differentiation of human fetal brain-derived NSCs (hNSCs) and to identify the fates of differentiated cells. When hNSCs were placed under proliferation or differentiation conditions in five media, proliferating and differentiating hNSCs exhibited different frequency and time dependences of capacitance, indicating that the proliferation and differentiation status of hNSCs may be discriminated in real-time using our capacitance sensor. In addition, comparison between real-time capacitance and time-lapse optical images revealed that neuronal and astroglial differentiation of hNSCs may be identified in real-time without cell labeling.

Human neural stem cells (hNSCs), which can give rise to neuronal or glial cells, have received considerable attention for their therapeutic potential to repair neural injury or dysfunction caused by trauma, stroke, and neurodegenerative diseases¹. For cell-replacement therapies, hNSCs could be differentiated into the appropriate neural cell types prior to transplantation, since pre-differentiated cells could be more therapeutically beneficial and undifferentiated hNSCs may remain immature or produce unwanted neural cell types after transplantation into the damaged or diseased brain²⁻⁵. Hence, it is important to monitor the process of *in vitro* hNSC differentiation and to identify specific differentiated cell fates. The fates of differentiated cells are usually identified via real-time polymerase chain reaction⁶ or immunohistochemical methods⁷ that involve labeling with nucleic acids or antibodies. However, these methods are invasive and time-consuming. We have therefore developed an alternative approach to monitor the differentiation of hNSCs and to identify the fate potential of differentiated hNSCs in real-time without cell labeling.

To monitor the differentiation of stem cells in real-time, electric cell-substrate impedance sensors have been used⁸⁻¹¹, which measure the alternating current (AC) impedance between a small sensing electrode and a large counter electrode while cells are cultured on the gold-sensing electrode. Cells attach and spread on the surface of the sensing electrode and passively block the current, and thus the electrode impedance is affected by the shape, adhesion, and/or mobility of adherent cells^{12,13}. However, compared to the electrode impedance, the capacitance (or the dielectric constant) of cells provides more direct information on cellular activities¹⁴⁻¹⁷; the fate potential of NSCs was previously reported to be more closely related to cell membrane capacitance than to conductance¹⁸. On this study, we have developed a capacitance sensor to monitor the differentiation of hNSCs. In our capacitance sensor, the cells are placed between the two electrodes rather than on top of the electrodes, and the change in capacitance is measured. Since the cells are placed between two electrodes, optical images of the cells and measurements of real-time capacitance can be obtained simultaneously, enabling a better understanding of hNSC differentiation.

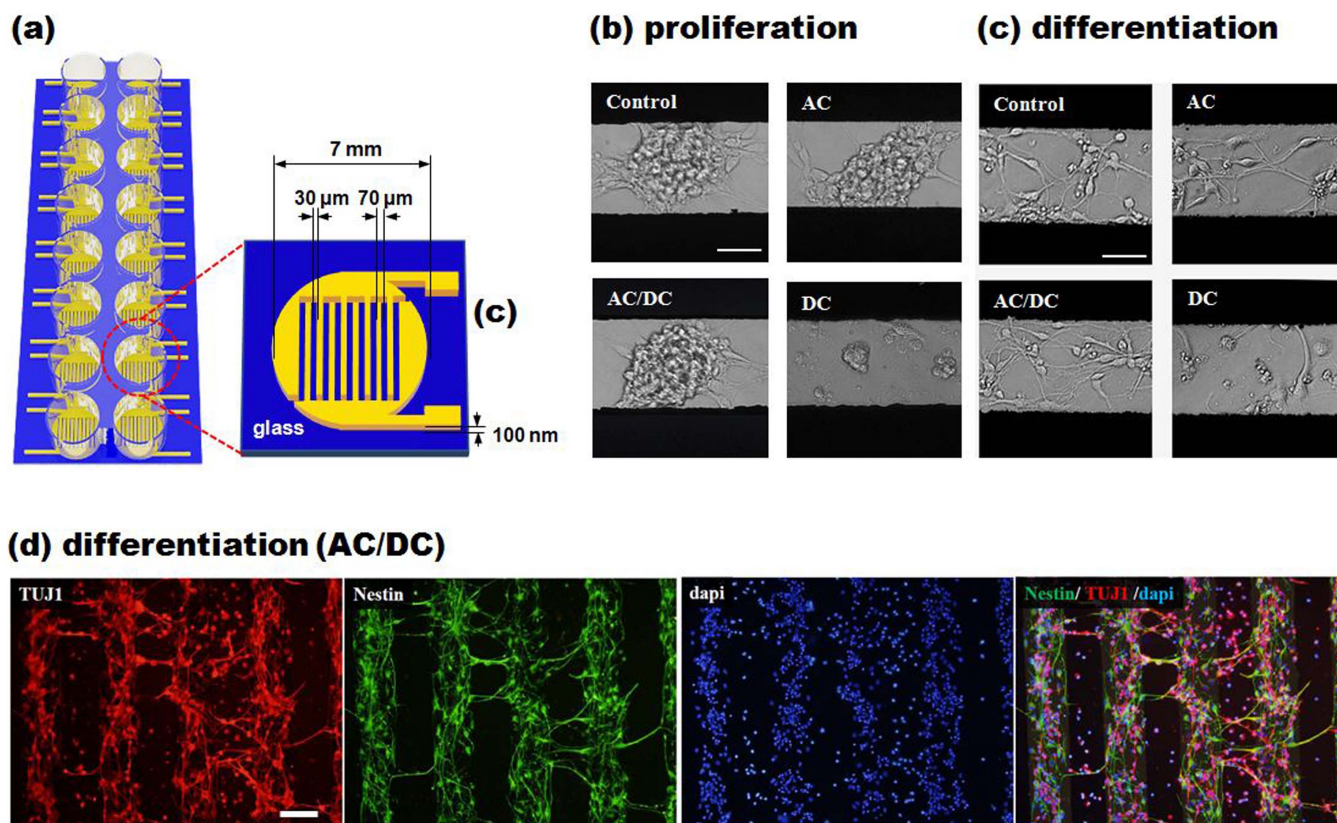


Figure 1 | Schematics of the capacitance array sensor and imaging cells in a sensor. (a) Schematic of a fabricated capacitance sensor (left) and diagram of a capacitance sensor with a gap of 30 μm and interface of 100 μm (right). (b, c) Optical images of hNSCs under (b) proliferation and (c) differentiation conditions in the non-stimulated control condition, and following to exposure to electric fields of AC, DC, or AC/DC. Scale bar is 50 μm .

(d) Five days after plating neurosphere-derived single cells onto the interdigitated electrodes, the differentiation of fractions of hNSCs exposed to AC/DC into TUJ1⁺ neurons was visualized by Texas Red and by the staining of nestin⁺ immature cells with fluorescein labeling. Nuclei were stained with DAPI. Scale bar is 100 μm .

Results

Prior to real-time monitoring of the differentiation of hNSCs using a capacitance sensor, we investigated the effect of electric fields on the proliferation and differentiation of hNSCs. hNSCs were placed on the interdigitated electrodes (Figure 1a), and then AC electric fields ($V_{\text{peak}} = 100 \text{ mV}$) and/or direct current (DC) electric fields (15 mV) were applied while hNSCs were maintained under proliferation or differentiation conditions. Compared to hNSCs without electric fields as a control, hNSCs were nearly unaffected by AC, while DC induced cell death substantially under both proliferation and differentiation conditions (Figures 1b and 1c), which is consistent with previously reported results^{19–22}. However, when DC was applied with AC (AC/DC), the cells appeared to proliferate or differentiate well (Figures 1b and 1c); moreover, some neurite extensions from differentiated cells seemed to align along the direction of the DC (Figure 1c).

We estimated the cell viability of hNSCs growing under proliferation or differentiation conditions in different electrical fields using a caspase-3 activity assay (Supplementary Fig. S1). As expected from the morphological findings (Figures 1b and 1c), higher caspase-3 activities were observed for cells exposed to DC than for control cells, indicating that significant apoptosis of hNSCs under both proliferation and differentiation conditions was induced by DC. This DC-induced decreased viability of hNSCs may be understood in terms of mass transport electrokinetically driven by DC; mass transport is reduced by DC, but enhanced by AC^{23,24}. In contrast, AC and AC/DC caused no significant difference in the caspase-3, haemocytometer live cell count, and TUJ1 activity versus control cells

(Supplementary Fig. S1), confirming that hNSC proliferation and differentiation were nearly unaffected by exposure to AC or AC/DC.

To visualize the neurite outgrowth in detail, hNSCs under differentiation conditions in AC/DC were immunostained with anti-TUJ1 and anti-hNestin antibodies (Figure 1d). Most TUJ1⁺ neurites from differentiated cells grew perpendicular to the direction of DC on the gold electrodes, as previously reported by Ariza et al.²¹. However, neurites between electrodes formed parallel to the DC direction, probably due to the neuronal migration along the direction of DC^{24,25}. Most TUJ1⁺ early neurons or neuroblasts also expressed nestin, suggesting that they may persist as immature precursor cells despite early neuronal differentiation (Figure 1d). Nestin, in particular, has been found to co-localize with newly committed neuroblasts or glial markers, including TUJ1 in hNSCs²⁶.

Next, we sought to monitor the differentiation of hNSCs and to identify specific differentiated cell fates in real-time without cell labeling. hNSCs were cultured in four media: proliferation medium (PM), PM without additional mitogenic stimulation factors (DM), DM containing 300 ng/mL of human noggin (NDM), and DM containing 20 ng/mL of bone morphogenetic protein 4 (ADM). hNSCs grown in DM gave rise to neuronal or glial cells. However, most hNSCs differentiated into astroglial cells in ADM, and predominantly differentiated into neurons in NDM at the expense of glial differentiation^{27–29}. To verify the differentiation patterns of hNSCs, neurosphere-derived single cells cultured for 5 days in the four media were immunostained with various cell markers (Figure 2). The population of TUJ1⁺ neurons was significantly larger in NDM than in DM or ADM, while the population of GFAP⁺ or S100 β ⁺ cells were not-

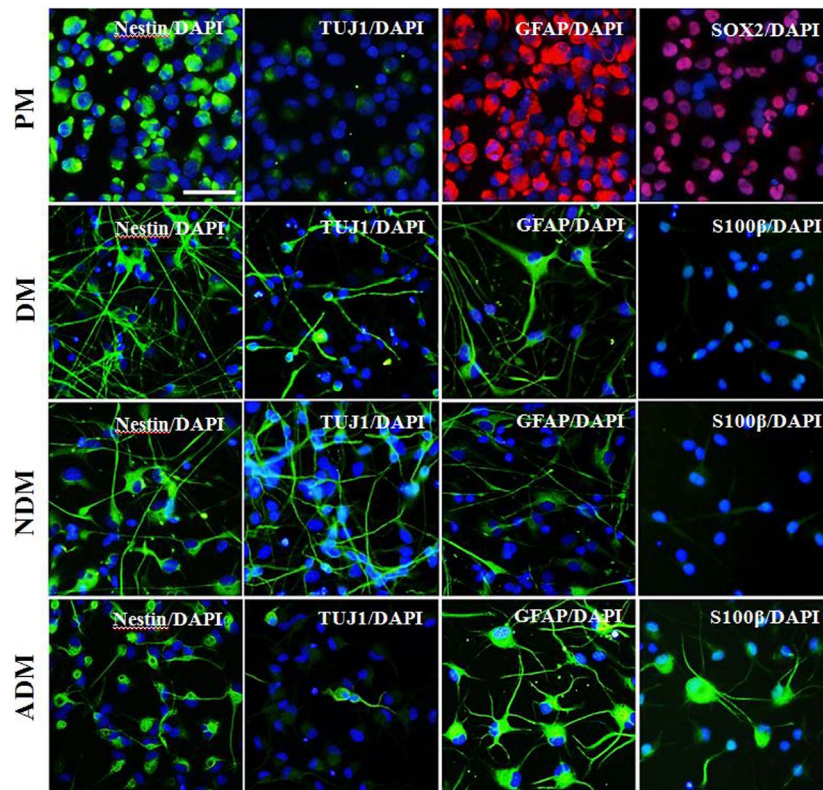


Figure 2 | Differentiation patterns of hNSCs in culture. Five days after plating neurosphere-derived single cells in DM, NDM, or ADM, fractions of hNSCs differentiated into TUJ1⁺ neurons, GFAP⁺ immature cells and/or astrocytes, and nestin⁺ immature cells were visualized via fluorescein labeling. In contrast, most hNSCs cultured in PM were co-labeled with nestin (green), SOX2 (red), and GFAP (red). Nuclei were stained with DAPI. Scale bar is 50 μ m.

ably larger in ADM than in DM or NDM. More than 70% of hNSCs differentiated into early neurons in NDM, while \sim 90% of hNSCs differentiated into astrocytes with appropriate morphology in ADM (Figures 2 and Supplementary Fig. S2). In addition, most hNSCs cultured in PM remained immature stem/progenitor cells expressing nestin, SOX2, and GFAP (Figure 2).

To determine whether the proliferation and differentiation status of hNSCs could be discriminated using our capacitance sensor, we measured capacitance as a function of frequency (f) while hNSCs were maintained under proliferation or differentiation conditions in various media (Figure 3a). When the cells grew under proliferation conditions in PM, the capacitance was fitted to the relationship of $C \propto f^{-\alpha}$ with $\alpha \approx 0.26$. In contrast, when the cells existed under differentiation conditions, the capacitance followed the relationship $C \propto f^{-\alpha}$ with $\alpha \approx 0.26$ at low frequencies, but decreased more rapidly at high frequencies. For confirmation of these observations, we measured the frequency dependence of the capacitance at various time points; similar behaviors occurred during hNSC proliferation or differentiation, although the measured capacitance values differed at different time points. We also measured the frequency dependence of the capacitance for the sensors with different concentrations of cells under differentiation conditions (Supplementary Fig. S3a). Similar frequency dependence was observed independently of the cell concentrations, indicating that the frequency dependence of the capacitance was not affected by the cell coverage of the sensor. The real-time capacitance was measured at 5 kHz while hNSCs were under proliferation or differentiation conditions in various media (Figure 3b). The measured capacitance (C) was normalized to the initial value (C_0) since C_0 was slightly different for different sensors. Under proliferation conditions in PM, the capacitance increased steadily due to increases in cell size and number (Supplementary Fig. S4) and became nearly constant after \sim 4.5 days, as previously reported^{14–17}. When the cells grew under differentiation conditions,

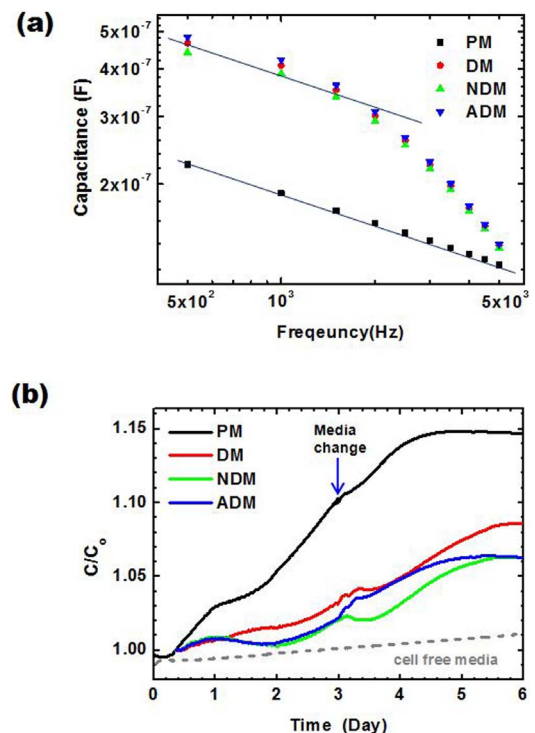


Figure 3 | Capacitance measurements of hNSCs. (a) Frequency dependence of capacitance for hNSCs under proliferation and differentiation conditions in PM, DM, NDM, or ADM. (b) Time dependence of normalized capacitance at 5 kHz for hNSCs in PM, DM, NDM, or ADM for 6 days. Culture medium was changed at the third day of incubation (blue arrow).

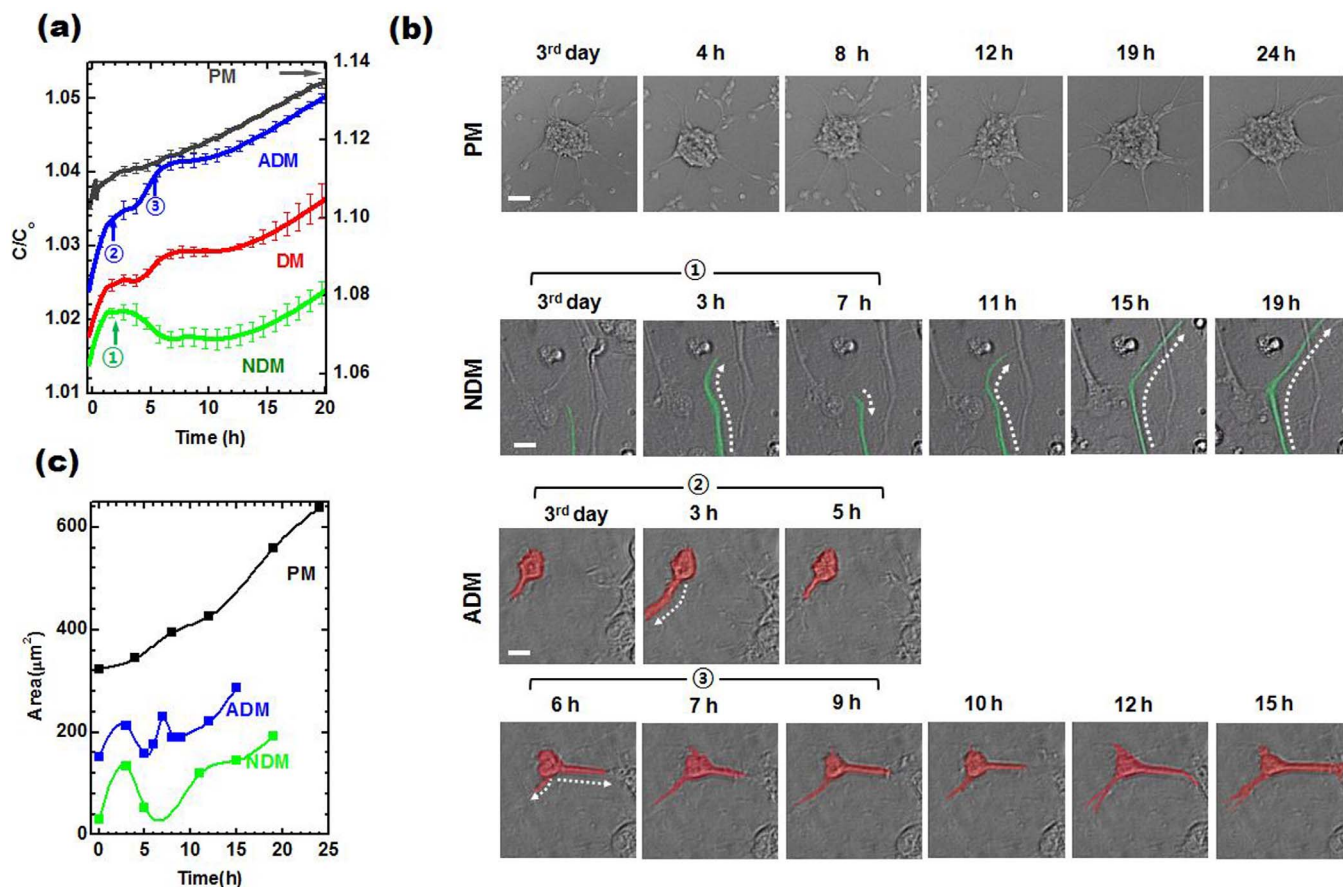


Figure 4 | Comparison of real-time capacitance and time-lapse images. (a) Real-time capacitance of hNSCs incubated in PM, DM, NDM, or ADM after refreshing the culture medium. The scale of PM is on the right side. Data represent mean \pm sem ($n = 3$). (b) Time-lapse optical images of hNSCs under proliferation condition in PM, differentiation conditions in NDM or ADM. The color-filled shapes represent the cell body (red) and cellular processes (green). Scale bar is 10 μm . (c) Area occupied by hNSCs under proliferation condition in PM, differentiation conditions in NDM or ADM, which is estimated from the time-lapse optical images.

the capacitance also increased, but the rate of increase was much slower than that of the cells grown under proliferation conditions (Supplementary Figs. S3b and S3d). Moreover, capacitance peaks were observed after the culture medium was changed on the third day (Figure 3b). Taken together, these results suggest that our capacitance sensor distinguishes between proliferating and differentiating hNSCs in real-time.

To investigate the observed capacitance peaks in more detail, real-time capacitance was measured after medium change (Figure 4a). When the cells were differentiated in DM or ADM, two small capacitance peaks occurred at 3 h and 8 h, although the first peak was smaller than the second one in ADM. On the other hand, when the cells were differentiated in NDM, only one large capacitance peak appeared at ~ 3 h. Time-lapse optical images (Figure 4b) were taken simultaneously with the real-time capacitance measurements after medium change on the third day. In PM, the cells aggregated to a cell cluster, and its volume increased (first column in Figure 4b). In NDM, however, a single neurite grew up to 3 h and then shrank, followed by regrowth (second column in Figure 4b). In ADM, a short astroglial process grew to 3 h and then shrank, similar to the behavior observed in NDM (third column in Figure 4b). However, the length of the glial process increased again from 6 h to 7 h, decreased slightly at 10 h, and then cell gradually manifested process-bearing, stellate astroglial morphology (fourth column in Figure 4b).

Comparison of time-lapse images and real-time capacitance suggested that the capacitance increased with increasing length of neuronal or glial processes; the capacitance peak formed as the extending neural process was transiently retracted after the change of medium.

Growth cones, the highly sensory and motile structures at the tips of growing neurites, guide axons toward their targets by responding to molecular cues in the environment^{30,31}. Changing the culture medium temporarily affects the extracellular signals sensed by growth cones, including physical and chemical conditions such as temperature, pH, ions, and growth factors, which cause the axon to retract, turn, and branch. Therefore, the first and second capacitance peaks in Figure 4a were due to the elongation and retraction of the outgrowing processes of differentiating neuronal and astroglial cells. Moreover, the time-lapse images demonstrated that growth of the axonal neurite underwent a series of rapid periods of elongation punctuated by stationary periods. Ultimately, the axonal neurite extended to some distance from the neuronal cell body, while the astroglial processes underwent short extension or retraction, but little net growth. From the time-lapse optical images, the area occupied by hNSCs incubated in PM, NDM, or ADM, was estimated using ImageJ software (Figure 4c). As for the real-time capacitance, one and two peaks were observed during differentiation in NDM and ADM, respectively, supporting that the different growth patterns of developing neuronal astroglial processes may generate one large capacitance peak during neuronal differentiation in NDM (first capacitance peak in Figure 4a) and two small capacitance peaks during astroglial differentiation in ADM (first and second capacitance peaks in Figure 4a). Based on these results, we conclude that the neuronal or astroglial fate of differentiated hNSCs may be identified with our capacitance sensor in real-time without cell labeling.

To confirm that the capacitance peak height is related to the neurite length, hNSCs were pre-exposed to 2 mM valproic acid for

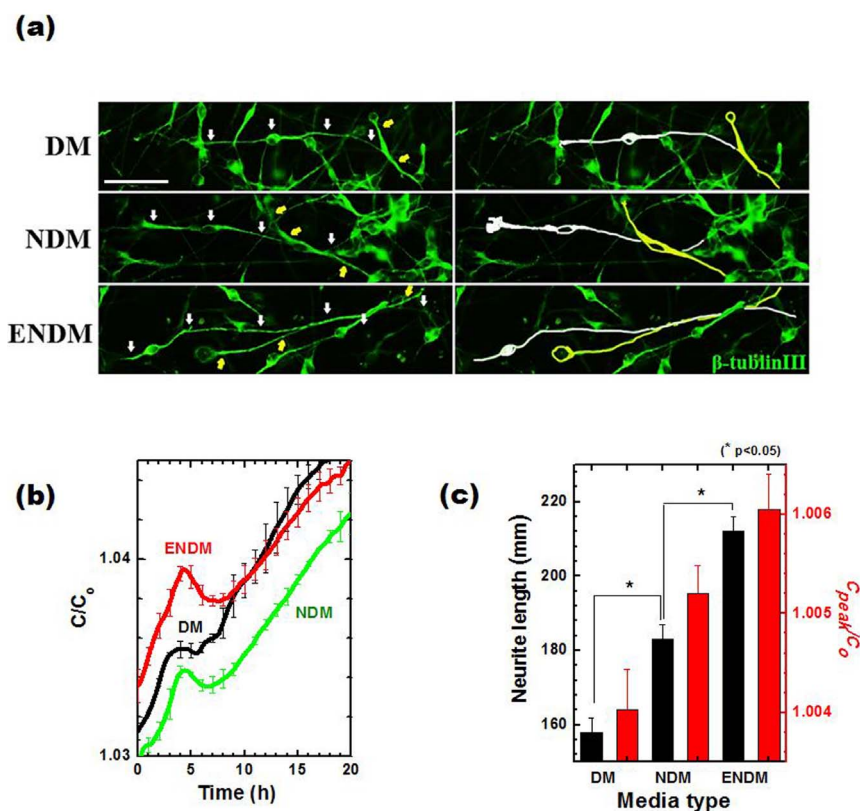


Figure 5 | Relationship between neurite length and real-time capacitance of hNSCs under differentiation conditions. (a) Five 5 days after plating neurosphere-derived single cells in DM, NDM, or ENDM, the differentiation of fractions of hNSCs into TUJ1⁺ neurons was visualized via fluorescent labeling. White and yellow arrows point to bipolar neuronal processes derived from two neuronal cell bodies (left panel). The shape of each neuronal process is depicted in white and yellow to aid visualization (right panel). Scale bar is 50 μm . (b) Real-time capacitance data of hNSCs incubated in DM, NDM, or ENDM after refreshing the medium. Data represent mean \pm sem ($n = 3$). (c) Quantification of neurite length by ImageJ and capacitance peak height for hNSCs in DM, NDM, or ENDM. Data represent mean \pm sem ($n = 3$).

4 h and then cultured under differentiation conditions in NDM (ENDM) since treatment with valproic acid was previously reported to enhance neurite elongation¹⁵. Immunofluorescence images of cells stained with anti-TUJ1 antibody showed that neurites were longer in ENDM than in NDM (Figures 5a and 5c). Real-time capacitance was measured while hNSCs were differentiated in DM, NDM, or ENDM (Figure 5b and Supplementary Fig. S5). For all media, the capacitance increased slightly during the first 3 days of culture and capacitance peaks were observed 3 h after medium change. However, the highest capacitance peak occurred in ENDM; the capacitance peak height was closely correlated with neurite length for three different media (Figure 5c). These findings indicate that the capacitance peak height increased with increasing neurite length, and that one large capacitance peak is related to neuronal differentiation from hNSCs.

Discussion

We have developed a label-free method to monitor the differentiation of hNSCs in real-time. While hNSCs grown under proliferation conditions displayed steady and rapid increases in capacitance without peak formation, hNSCs under differentiation conditions exhibited a slow increase in capacitance with peak formation, indicating that the proliferation and differentiation status of hNSCs can be distinguished in real-time. Comparison of real-time capacitance measurements and time-lapse optical images revealed that one large and two small capacitance peaks, which were observed after medium change, probably resulted from neuronal and astroglial differentiation from hNSCs, respectively. These results demonstrate that the fate potential of differentiated hNSCs may be identified in real-time by measuring capacitance change in growing cells. In addition, we

found that the differentiation and proliferation status of hNSCs was nearly unaffected by exposure to AC or to AC/DC.

Methods

Materials. Human brain tissue from an aborted fetus at 13 weeks of gestation was obtained with full parental consent and approval of the research ethics committee of Yonsei University College of Medicine, Seoul, Korea (protocol #4-2003-0078). This work was carried out in accordance with The Code of Ethics of the World Medical Association (Declaration of Helsinki).

For culturing hNSCs, Dulbecco's modified Eagle's medium and Ham's F12 medium with penicillin, streptomycin (1% v/v), and N2 formulation (1% v/v) were purchased from Gibco (Grand Island, NY, USA). To achieve mitogenic stimulation, leukemia inhibitory factor and heparin were obtained from Sigma (St. Louis, MO, USA), and fibroblast growth factor 2, human noggin, bone morphogenetic protein 4, and valproic acid were obtained from R&D Systems (Minneapolis, MN, USA).

For immunocytochemistry, the following antibodies were purchased: anti-human-specific nestin (anti-hNestin; 1 : 200, Chemicon, Temecula, CA, USA), anti-neuronal class β -tubulin III (TUJ1; 1 : 1000, Covance, Princeton, NJ, USA), anti-glial fibrillary acidic protein (GFAP; 1 : 1000, Dako, Glostrup, Denmark), anti-S100 β (1 : 1000, Sigma), anti-microtubule-associated protein 2 (MAP2; 1 : 50, Cell Signaling Technology, Danvers, MA, USA), anti-SOX2, (1 : 1000, Chemicon). Secondary antibodies were conjugated with fluorescein (1 : 180, Vector, Burlingame, CA, USA) or Texas Red (1 : 180, Vector), 4,6-diamino-2-phenylindole (DAPI; Vector), and propidium iodide/RNase staining buffer (BD Biosciences, Heidelberg, Germany) were also obtained.

Cell culture. hNSCs derived from a single donated fetal telencephalic brain tissue were cultured and maintained as neurospheres in proliferation medium (PM). PM consisted of Dulbecco's modified Eagle's medium and Ham's F12 supplemented with penicillin/streptomycin (1% v/v) and N2 formulation (1% v/v) at a 1 : 1 volume ratio. It also included mitogenic stimulation factors such as fibroblast growth factor 2 (20 ng/mL), leukemia inhibitory factor (10 ng/mL), and heparin (8 $\mu\text{g/mL}$). For the induction of differentiation, hNSCs were cultured in four media: PM without additional mitogenic stimulation factors (DM), DM containing 300 ng/mL of human noggin (NDM), DM containing 20 ng/mL of bone morphogenetic protein 4 (ADM),



and DM containing 2 mM of valproic acid (ENDM). All cultures were maintained in a humidified incubator at 37°C and 5% CO₂ in air, and half of the growth medium was replenished every third day.

Immunocytochemistry. To identify the differentiation patterns of hNSCs, neurospheres were trypsinized and dissociated into single cells, and 8×10^4 cells were placed on poly-L-lysine (10 µg/mL, Sigma)-coated 8-well chamber slides (Nunc, Roskilde, Denmark) and cultured in PM, DM, NDM, ENDM, or ADM. Medium was replaced every second day. The medium was removed 1 week after plating, and the cells were fixed with 4% paraformaldehyde in PIPES buffer (Sigma), rinsed with phosphate-buffered saline, blocked with 3% bovine serum albumin (Sigma), 10% normal horse serum, and 0.3% Triton X-100 (Sigma) in phosphate-buffered saline, and incubated with the following primary antibodies: anti-hNestin as a neural stem/progenitor marker, anti-TUJ1 as an early neuronal marker, anti-GFAP as a neural stem/progenitor or astrocyte marker, anti-S100β as an astrocyte marker, anti-MAP2 as a mature neuronal marker, and anti-SOX2 as a neural stem/progenitor marker. Next, the cells were incubated with species-specific secondary antibodies, conjugated with fluorescein or Texas Red, and mounted using Vectashield mounting medium (Vector) with DAPI. The stained cells were examined by immunofluorescence microscopy (BX51, Olympus, Center Valley, PA, USA). The percentage of cells positive for each antigen was determined and compared to the total number of cells labeled with DAPI.

For measuring caspase-3 activity, hNSCs under proliferation and differentiation conditions in different electrical fields were immunostained with anti-cleaved caspase-3 antibody (1 : 500, BD Pharmingen, CA, USA) at 3 days after plating. Active caspase-3 was labeled by use of rabbit IgG-FITC (1 : 180, Vector) and the nucleus was stained by DAPI. Images were obtained using immunofluorescence microscopy.

Fabrication of capacitance sensor array. A capacitance sensor array consisting of 16 sensors with interdigitated electrodes was fabricated on a glass substrate (Figure 1a). A gold electrode (100 nm thick) with a gap size of 30 µm was patterned using photolithography and lift-off techniques. For cell culture, acrylic wells (LOT# 10118564; Thermo) were attached to the array sensor with a curing agent (polymethylsiloxane and toluene mixed at 1 : 10). Prior to cell seeding, the capacitance sensor array was sterilized in an autoclave and then coated with poly-L-lysine.

Measurements. For the inoculation of cells, 200 µL of cell suspension (2×10^5 cells/mL) were transferred into each well of the capacitance sensor array, resulting in a final surface concentration of 4×10^4 cells/cm². For the induction of proliferation or differentiation of hNSCs, the capacitance sensor array was placed inside an incubator maintained at 37°C under an atmosphere of 5% CO₂. The capacitance was measured using an LCR meter (Agilent 4294A, CA, USA) with an AC voltage of 100 mV at frequencies ranging from 500 Hz to 5 kHz. The sensor inside the incubator and the LCR meter outside the incubator were linked via electrical connectors mounted on the side of the incubator. Capacitance was measured simultaneously from all 16 sensors with a data acquisition/switching unit (Agilent 34970A) connected to the LCR meter. Data were collected every 5 min for each sensor. To obtain time-lapse optical images, the cells were incubated in a Chamlide™ chamber (Live Cell Instrument) maintained at 37°C under an atmosphere of 5% CO₂.

Statistical analysis. The statistic software SPSS18.0 (IBM, NY, USA) was used for data analysis. Values are reported as mean ± standard error mean (sem). Statistical differences were assessed either by a non-parametric Mann-Whitney U test or a non-parametric one-way Kruskal-Wallis test.

1. Horner, P. J. G. & Fred, H. Regenerating the damaged central nervous system. *Nature* **407**, 963–970 (2000).
2. Faulkner, J. R. *et al.* Reactive Astrocytes Protect Tissue and Preserve Function after Spinal Cord Injury. *J. Neurosci.* **24**, 2143–2155 (2004).
3. In Park, K. *et al.* Acute injury directs the migration, proliferation, and differentiation of solid organ stem cells: Evidence from the effect of hypoxia-ischemia in the CNS on clonal “reporter” neural stem cells. *Exp. Neurol.* **199**, 156–178 (2006).
4. Kim, H. O. *et al.* Selective Depletion of SSEA-3- and TRA-1-60-Positive Undifferentiated Human Embryonic Stem Cells by Magnetic Activated Cell Sorter (MACS). *Tissue Eng. Regen. Med.* **8**, 253–261 (2011).
5. Okada, S. *et al.* Conditional ablation of Stat3 or Socs3 discloses a dual role for reactive astrocytes after spinal cord injury. *Nat. Med.* **12**, 829–834 (2006).
6. Noaksson, K. *et al.* Monitoring Differentiation of Human Embryonic Stem Cells Using Real-Time PCR. *Stem Cells* **23**, 1460–1467 (2005).
7. Hill, D. P. & Robertson, K. A. Differentiation of LA-N-5 neuroblastoma cells into cholinergic neurons: methods for differentiation, immunohistochemistry and reporter gene introduction. *Brain Res. Protoc.* **2**, 183–190 (1998).
8. Bagnaninchi, P. O. & Drummond, N. Real-time label-free monitoring of adipose-derived stem cell differentiation with electric cell-substrate impedance sensing. *Proc. Natl. Acad. Sci. USA* **108**, 6462–6467 (2011).
9. Reitingner, S., Wissenwasser, J., Kapferer, W., Heer, R. & Lepperdinger, G. Electric impedance sensing in cell-substrates for rapid and selective multipotential differentiation capacity monitoring of human mesenchymal stem cells. *Biosens. Bioelectron.* **34**, 63–69 (2012).

10. Zhang, Y., Wang, H., Wang, L. & Cheng, J. Real-Time, Label-Free Monitoring of 3T3-L1 Preadipocyte Differentiation by a Bioelectrical Impedance Assay. *Anal. Lett.* **45**, 1045–1057 (2012).
11. Park, H. E. *et al.* Real-Time Monitoring of Neural Differentiation of Human Mesenchymal Stem Cells by Electric Cell-Substrate Impedance Sensing. *J. Biomed. Biotechnol.* **2011**, 485173 (2011).
12. Pethig, R. Dielectric Properties of Biological Materials: Biophysical and Medical Applications. *IEEE T. Electr. Insul.* **EI-19**, 453–474 (1984).
13. Tirado, M., Grosse, C., Schrader, W. & Kaatz, U. Broad frequency range dielectric spectroscopy of aqueous suspensions of phospholipid vesicles. *J. Non-cryst. Solids* **305**, 373–378 (2002).
14. Lee, R. M., Choi, H., Shin, J.-S., Kim, K. & Yoo, K.-H. Distinguishing between apoptosis and necrosis using a capacitance sensor. *Biosens. Bioelectron.* **24**, 2586–2591 (2009).
15. Lee, R. *et al.* Capacitance-based real time monitoring of receptor-mediated endocytosis. *Biosens. Bioelectron.* **25**, 1325–1332 (2010).
16. Lee, R. *et al.* Capacitance-based assay for real-time monitoring of endocytosis and cell viability. *Lab. Chip* **12**, 2377–2384 (2012).
17. Lee, R., Jung, I., Park, M., Ha, H. & Yoo, K. H. Real-time monitoring of adipocyte differentiation using a capacitance sensor array. *Lab. Chip* **13**, 3410–3416 (2013).
18. Labeed, F. H. *et al.* Biophysical characteristics reveal neural stem cell differentiation potential. *PLoS One* **6**, e25458 (2011).
19. Matos, M. A., White, L. R. & Tilton, R. D. Enhanced mixing in polyacrylamide gels containing embedded silica nanoparticles as internal electroosmotic pumps. *Colloid. Surface B* **61**, 262–269 (2008).
20. Zhao, M. Electrical fields in wound healing—An overriding signal that directs cell migration. *Semin. Cell Dev. Bio.* **20**, 674–682 (2009).
21. Ariza, C. *et al.* The Influence of Electric Fields on Hippocampal Neural Progenitor Cells. *Stem Cell Rev. Rep.* **6**, 585–600 (2010).
22. Yao, L., Pandit, A., Yao, S. & McCaig, C. D. Electric field-guided neuron migration: a novel approach in neurogenesis. *Tissue Eng. Pt. B- Rev.* **17**, 143–153 (2011).
23. Matos, M. A. & Cicerone, M. T. Alternating current electric field effects on neural stem cell viability and differentiation. *Biotechnol. Progr.* **26**, 664–670 (2010).
24. McCaig, C. D. Dynamic aspects of amphibian neurite growth and the effects of an applied electric field. *J. Physiol.* **375**, 55–69 (1986).
25. McCaig, C. D. Spinal neurite reabsorption and regrowth in vitro depend on the polarity of an applied electric field. *Development* **100**, 31–41 (1987).
26. Fanarraga, M. L., Avila, J. & Zabalá, J. C. Expression of unphosphorylated class III β-tubulin isotype in neuroepithelial cells demonstrates neuroblast commitment and differentiation. *Eur. J. Neurosci.* **11**, 517–527 (1999).
27. Lim, D. A. *et al.* Noggin Antagonizes BMP Signaling to Create a Niche for Adult Neurogenesis. *Neuron* **28**, 713–726 (2000).
28. Mehler, M., Mabie, P. C., Zhu, G., Gokhan, S. & Kessler, J. A. Developmental changes in progenitor cell responsiveness to bone morphogenetic proteins differentially modulate progressive CNS lineage fate. *Dev. Neurosci.* **22**, 74–85 (2000).
29. Poumay, Y. & Pittelkow, M. R. Cell density and culture factors regulate keratinocyte commitment to differentiation and expression of suprabasal K1/K10 keratins. *J. Invest. Dermatol.* **104**, 271–276 (1995).
30. Tessier-Lavigne, M. & Goodman, C. S. The molecular biology of axon guidance. *Science* **274**, 1123–1133 (1996).
31. Dickson, B. J. Molecular mechanisms of axon guidance. *Science* **298**, 1959–1964 (2002).

Acknowledgments

This work was financially supported by MEST through the National Research Foundation (NRF) of Korea (NRF-2012R1A4A1029061, NRF-2011-0017486, NRF-2013R1A1A304009309, and NRF-2013M3A9B4076545), Brain Korea 21 Plus Project for Physics, MHW through the Korean Health Technology R&D Project (Grant No. A110905, and A121943), and the Faculty Grant of Yonsei University College of Medicine (6-2006-0017).

Author contributions

R.L. fabricated interdigitated capacitance array sensor and measured the capacitance of hNSCs. N.H. measured hNSCs response to AC and/or DC electric field stimulation. I.S.K. and S.Y. performed immunocytochemistry. K.H.Y. and K.I.P. designed the experiment and wrote the manuscript.

Additional information

Supplementary information accompanies this paper at <http://www.nature.com/scientificreports>

Competing financial interests: The authors declare no competing financial interests.

How to cite this article: Lee, R. *et al.* Real-Time Discrimination between Proliferation and Neuronal and Astroglial Differentiation of Human Neural Stem Cells. *Sci. Rep.* **4**, 6319; DOI:10.1038/srep06319 (2014).



This work is licensed under a Creative Commons Attribution-NonCommercial-NoDerivs 4.0 International License. The images or other third party material in this article are included in the article's Creative Commons license, unless indicated otherwise in the credit line; if the material is not included under the Creative

Commons license, users will need to obtain permission from the license holder in order to reproduce the material. To view a copy of this license, visit <http://creativecommons.org/licenses/by-nc-nd/4.0/>